High Power Laser Science and Engineering, (2025), Vol. 13, e54, 12 pages.
doi:10.1017/hpl.2025.19

HIGH POWER LASER SCIENCE AND ENGINEERING

REVIEW

Femtosecond precision synchronization system for SHINE

Bowei Wu[1,3], Jinguo Wang[2], Wenyan Zhang[2], Lie Feng[2], Xingtao Wang[2], and Bo Liu[2]

[1] *Shanghai Institute of Applied Physics, Chinese Academy of Sciences, Shanghai, China*

[2] *Shanghai Advanced Research Institute, Chinese Academy of Sciences, Shanghai, China*

[3] *University of Chinese Academy of Sciences, Beijing, China*

(Received 15 November 2024; revised 20 December 2024; accepted 20 February 2025)

Abstract

This paper presents a detailed technical overview of the femtosecond precision timing and synchronization systems implemented at the Shanghai high repetition rate XFEL and extreme light facility (SHINE). These systems are designed to deliver stabilized optical references to multiple receiver clients, ensuring high-precision synchronization between the optical master oscillator (OMO) and optical/RF subsystems. The core components include an OMO, fiber length stabilizers and laser-to-laser synchronization modules that achieve femtosecond-level accuracy. Our discussion extends to the various subsystems that comprise the synchronization infrastructure, including the OMO, fiber length stabilizer and advanced phase detection techniques. Finally, we highlight ongoing research and development efforts aimed at enhancing the functionality and efficiency of these systems, thereby contributing to the advancement of X-ray free-electron laser technology and its applications in scientific research.

Keywords: optical synchronization; SHINE; synchronization of large accelerator facilities

1. Introduction

X-ray free-electron lasers (XFELs) represent a revolutionary class of light sources, known as one type of the fourth-generation light sources[1–3]. These devices generate ultra-short, ultra-intense and coherent X-ray pulses with high-energy electron beams in strong periodical magnetic fields. XFELs exhibit peak brightness up to 10^9 times higher than traditional synchrotron radiation sources, with pulse widths at the femtosecond level[4,5]. Their spectral range spans from hard X-rays to soft X-rays, and they possess a high degree of beam coherence. These characteristics make XFELs invaluable for advancing basic research and high-tech development in fields such as material science, life science and energy science[6–9].

For large-scale scientific facilities such as XFELs, which span several hundred meters to kilometers, precise synchronization between various components is of paramount importance. In the case of XFELs, it is essential to ensure long-term stable synchronization among the photo-injector lasers, seed lasers, low-level radio frequency (RF) systems, beam diagnostics and probe lasers[10–13]. Some of these systems require time jitter to be maintained below 10 fs[14]. To meet the high precision and stability demands of synchronization in such large scientific facilities, a femtosecond timing and synchronization system is indispensable[15]. Typically, a femtosecond synchronization system must encompass three types of critical components. Firstly, it requires a low-noise master oscillator (OMO) to provide a stable reference. Secondly, it must be ensured that the reference can be transmitted to remote locations with ultra-low jitter and drift through stabilized links. Finally, the system must achieve high-precision phase synchronization between the reference and remote RF or optical subsystems. To address these challenges, major research institutions and XFEL facilities worldwide have made significant efforts and proposed various solutions, which include FLASH[15,16], the European XFEL[17,18], LCLS[2,19,20], SwissFEL[21,22], SACLA[23], FERMI[24], PAL-XFEL[25], SXFEL[26,27] and SHINE[4] (under construction).

This paper introduces the fundamental principles and components of the femtosecond synchronization system for SHINE, discussing the current research status and potential engineering challenges of large-scale femtosecond

Correspondence to: B. Liu, Shanghai Advanced Research Institute, Chinese Academy of Sciences, No. 99 Haike Road, Zhangjiang Hi-Tech Park, Shanghai 201210, China. Email: bo.liu@sari.ac.cn

synchronization systems. We provide a detailed description of the OMO, the stabilized optical fiber link and the synchronization methods between the optical reference and laser and between optical reference and RF subsystems. The continuous development and refinement of these systems are crucial for the successful operation of SHINE.

2. Femtosecond synchronization system

Compared to the 532-m-long SXFEL, the under-construction SHINE facility extends to 3.1 km. Consequently, the original synchronization scheme is no longer adequate for such a large-scale accelerator facility. To meet the various synchronization requirements of the facility, we have redesigned and planned a femtosecond precision synchronization system for SHINE. The layout diagram of this system is shown in Figure 1. The system begins with the generation of ultra-low-noise optical pulse trains by a mode-locked laser, with a repetition rate of 216.67 MHz, which serves as the optical reference. This OMO is phase-locked with a 1.3 GHz (six times the OMO frequency) RF master oscillator (RMO) to ensure long-term stable operation.

The stable pulse train from the OMO is divided in the optical fiber distribution unit and guided to various fiber length stabilizers (FLSs) through polarization-maintaining fibers (PMFs). To minimize drift caused by temperature and relative humidity, both the OMO and the optical fiber distribution unit are housed in a temperature-stabilized platform (TSP). This ensures precise environmental stability control, with a root mean square (RMS) temperature stability of 0.013°C in 140 h. Subsequently, the optical reference pulses are distributed via PMFs to various critical RF and optical subsystems of the facility. To prevent time drift during transmission, dispersion-compensated and timing-stabilized fiber links, known as FLSs, are employed[27,28]. Each FLS actively stabilizes the effective length of its associated optical fiber link using piezoelectric fiber stretchers and optical delay lines, ensuring that the optical reference pulses are stably transmitted to the sites requiring femtosecond timing stability.

The laser pulse train can be directly used for diagnostic purposes, such as in the bunch arrival time monitor (BAM). This requires electro-optic modulation of the optical reference laser pulse by the associated transient transverse electric field to extract the relative arrival time of the electron beam, necessitating femtosecond-level precision[29,30]. In addition, the reference pulse can be used to achieve high-precision synchronization of various optical subsystems of the XFEL or external optical lasers through a two-color balanced optical cross-correlator (TC-BOC)[31–34]. A typical example is pump–probe experiments, which require synchronization precision of less than 10 fs between the pump laser and the XFEL. Furthermore, lasers such as the photoinjector laser, seed laser and electro-optic sampling laser also require synchronization precision ranging from picoseconds to femtoseconds[35–37]. Moreover, achieving high-precision synchronization between the laser pulses and RF signals is crucial for various RF subsystems. For instance, ultra-low jitter microwave signals can be extracted from the optical pulses through a balanced optical microwave phase detector (BOMPD), which is a promising method for generating high-quality microwave signals. This synchronization scheme is robust against photodetector nonlinearities and can achieve sub-10 fs timing jitter between the extracted RF signal and the pulse train[38].

3. Optical master oscillator

As the core of a femtosecond synchronization system, the master oscillator must provide an ultra-stable time reference. Different research institutions have proposed various solutions, including continuous wave (CW) lasers, mode-locked

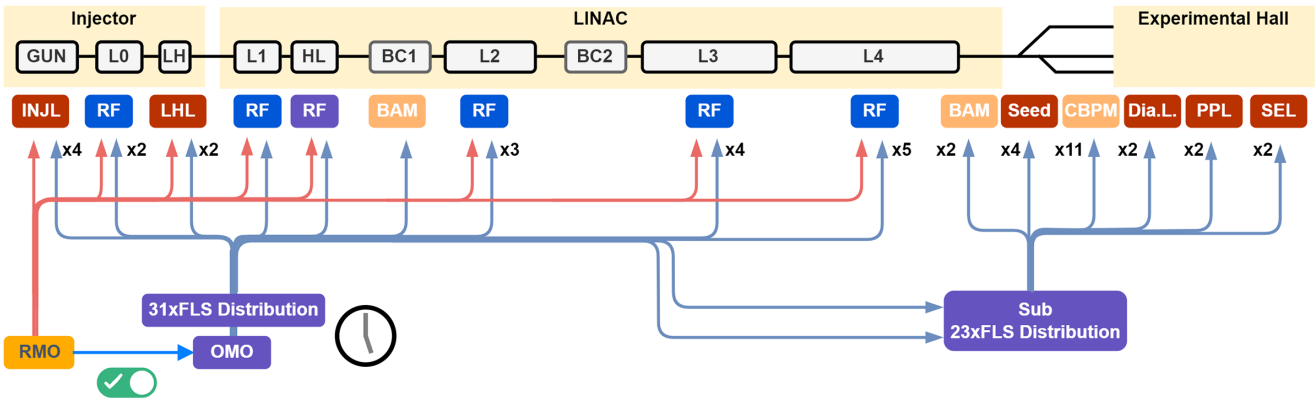

Figure 1. Schematic overview of the optical synchronization system for SHINE. L, LINAC; LH, laser heater; BC, bunch compressor; INJL, injector laser; LHL, heater laser; BAM, bunch arrival time monitor; CBPM, cavity beam position monitor; Dia.L., diagnostic laser; PPL, pump-probe laser; SEL, station of extreme light.

https://doi.org/10.1017/hpl.2025.19 Published online by Cambridge University Press

lasers and RF references. The current mainstream solution is to use mode-locked lasers, particularly those using erbium (Er) and erbium/ytterbium (Er/Yb)-doped gain media, as the master oscillators for large-scale XFEL facilities. Mode-locked lasers have the advantage of generating ultra-short pulses with high peak power, broad spectra and low timing jitter. This enables them to achieve sub-femtosecond resolution in corresponding optical–optical and optical–RF phase detection schemes, including balanced optical cross-correlators (BOCs) and BOMPDs. Such timing detection precision, typically in the range of femtoseconds to sub-femtoseconds[34,39], is difficult to achieve with other timing reference sources such as CW lasers or standard RF references, which usually operate with timing uncertainties on the order of picoseconds. Therefore, using low-noise mode-locked lasers as the OMO in XFEL femtosecond synchronization systems is the ideal choice to ensure the stable operation of the system.

The OMO for the femtosecond optical synchronization system used in SHINE is a commercial mode-locked laser from Menhir Photonics. This laser boasts excellent short-term stability and low phase noise, capable of emitting laser pulses at a wavelength of 1550 nm and a repetition rate of 216.67 MHz (one-sixth of the main RF cavity resonance frequency of 1.3 GHz). Due to environmental changes affecting the cavity length of the mode-locked laser, time drift can be introduced during 24/7 long-term operation. To ensure optimal long-term performance, a phase-locked loop (PLL) scheme[40] is employed to synchronize the OMO with the 1.3 GHz RMO.

For optical-to-RF synchronization, the direct detection method using photodiodes is a straightforward and widely adopted approach, particularly in scenarios where ultra-high precision is not critical[41–43]. However, this method is inevitably affected by amplitude-to-phase (AM-to-PM) conversion[44], which introduces significant phase noise and greatly impacts the phase detection accuracy and stability.

To overcome the limitations, SHINE employs a phase detector based on a Sagnac loop interferometer, which has a similar working principle with BOMPD[45,46] and fiber-loop optical–microwave phase detector (FLOMPD)[47]. This advanced phase detection technique provides femtosecond-level phase detection precision while minimizing sensitivity to external noise and environmental disturbances. The system's high-resolution phase measurement and robust noise suppression capabilities are crucial for achieving the ultra-stable timing required for SHINE's high-precision synchronization applications.

3.1. Femtosecond optical to microwave phase detector

The development of femtosecond-level phase detectors has seen significant advancements over recent decades, driven by the need for ultra-precise synchronization in applications like free-electron lasers and large-scale accelerators. Early phase detectors faced limitations with noise, especially due to AM-to-PM conversion. In 2004, Kim *et al*. introduced a setup that synchronized a 100 MHz Ti:sapphire laser with a 2 GHz RF signal, achieving timing jitter below 100 fs[48]. However, free-space setups were found to be less stable for long-term use. In response, Kim *et al*. proposed a fiber-based Sagnac loop design in 2006, formally introducing the BOMPD. This configuration improved phase stability by using counter-propagating optical pulses within the fiber loop to cancel out common-mode noise and reduce AM-to-PM conversion effects. The BOMPD achieved femtosecond precision, with an in-loop jitter of approximately 3 fs when synchronizing a 10.225 GHz voltage-controlled oscillator (VCO) with a stretched-pulse erbium-doped fiber laser operating at 44.26 MHz, demonstrating its efficacy in minimizing noise and drift over time[45]. Building on these developments, a new design called FLOMPD was introduced in 2012[47,49]. This configuration enhanced both short-term jitter and long-term drift control, achieving sub-femtosecond-level short-term phase noise and exceptional long-term phase stability. The FLOMPD's architecture leverages a stabilized fiber-loop design to further reduce phase noise and improve timing accuracy in optical-to-microwave synchronization systems, making it a preferred choice for high-precision phase stabilization in mode-locked fiber laser setups.

3.2. Optical to microwave phase detector based on a 3×3 coupler

Despite achieving very high phase detection accuracy, the free-space structure in this scheme can still impact the simplicity of the device. In Refs. [50,51], this scheme has been optimized by using a polarization-maintaining symmetric 3×3 coupler for biasing the Sagnac interferometer. In contrast to the 2×2 coupler architecture, which requires a nonreciprocal $\pi/2$ phase bias unit, the 3×3 coupler architecture has an inherent phase bias characteristic without additional bias units. This approach eliminates the need for magneto-optical components or complex RF electronic devices for Sagnac loop biasing, simplifying the structure while maintaining high stability and achieving sub-femtosecond resolution. The 3×3 coupler evenly splits the input into three output ports. The pulse outputs at these ports have a 'three-phase' relationship with the Sagnac phase, which is illustrated in Figure 2. In the Sagnac loop, two counter-propagating pulse trains experience different phase shifts, and the resulting interference signals are emitted at the output ports, each having a $2\pi/3$ phase relationship with one another. Similarly, a BPD is used to detect the two outputs of the Sagnac loop, generating a voltage signal that contains timing error information.

https://doi.org/10.1017/hpl.2025.19 Published online by Cambridge University Press

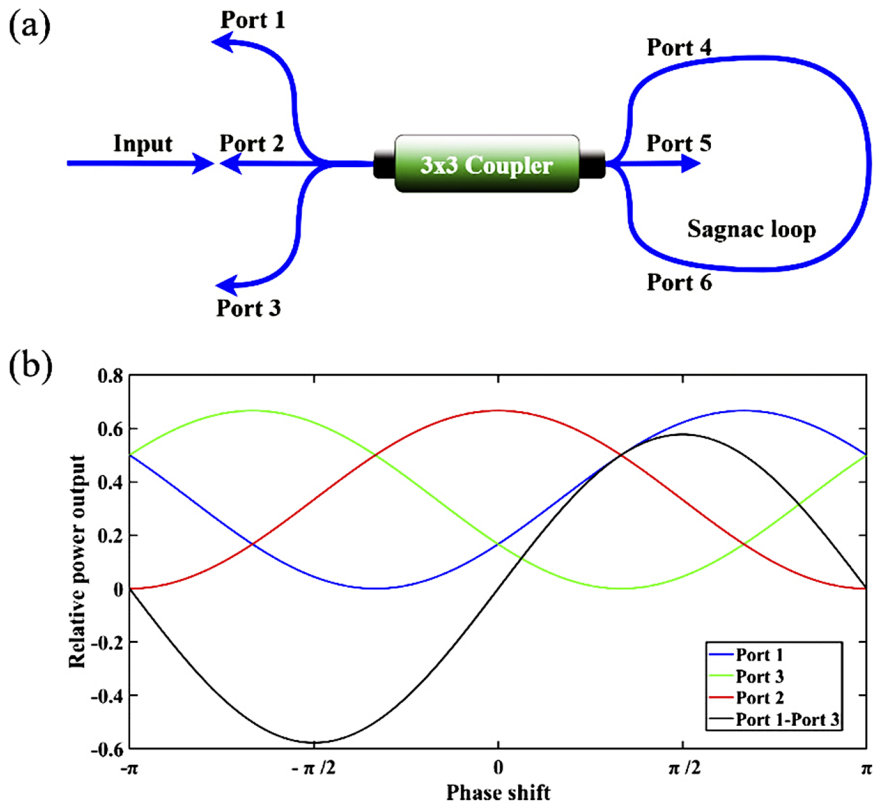

Figure 2. (a) Basic optical architecture of Sagnac loop interferometer by a 3×3 coupler. (b) Sagnac phase relationship of the three output ports.

In Ref. [50], we synchronized a 2.856 GHz microwave signal with a 238 MHz optical pulse train. Within a bandwidth range from 10 Hz to 10 MHz, this scheme achieved a relative timing jitter of 16 fs in the 10 Hz–10 MHz frequency offset range. This phase detection scheme has demonstrated significant application value. Compared with the original scheme, this scheme greatly simplifies the structure while maintaining excellent phase detection precision.

In our current work, we are optimizing this scheme and extending its application to the 1.3 GHz frequency used in SHINE. An experimental setup (shown in Figure 3) was constructed where a 3×3 coupler-based phase detector (shown in Figure 4(a)) phase-locks a 216.67 MHz mode-locked laser to a 1.3 GHz RF oscillator. The electronic phase-locking module used for this setup, shown in Figure 4(b), integrates the necessary control electronics within a compact enclosure to enhance system stability and minimize environmental noise. The phase-locking accuracy was assessed by implementing an identical out-of-loop phase detection setup to measure the residual timing jitter, confirming system stability. In this setup, the 1.3 GHz RF oscillator (Rohde & Schwarz, SMA100B) serves as the reference. Two nearly identical Sagnac-based phase detection setups were configured—one in-loop for phase-locking and the other out-of-loop for jitter evaluation. An optical delay line was introduced into the out-of-loop path for timing sensitivity calibration and balance-point adjustment. The experimental results (shown in Figure 5) demonstrate that within a bandwidth of 10 Hz to 10 MHz, the out-of-loop integrated RMS jitter of the synchronized optical oscillator is 4.9 fs, and the long-term RMS drift over 10 h is 5.56 fs, meeting the stringent timing stability required by SHINE.

4. Fiber link stabilization

Compared to the commercialized mode-locked lasers and RF master oscillators, as well as the relatively mature optoelectronic phase-locked loop technology, stabilizing the optical fiber link presents a significant challenge in achieving femtosecond-level synchronization. During the long-distance transmission of optical reference signals through fiber links, various environmental factors—such as temperature fluctuations, humidity changes, mechanical vibrations and pressure variations—can alter the physical and optical properties of the fiber, leading to optical delay variations. For instance, in a laboratory environment setting with a 300-m-long optical fiber, such environmental variations can result in a time drift of up to 4.5 ps within 100 s[52,53]. Additionally, in accelerator environments like tunnels, where the ambient temperature can fluctuate significantly over time, these effects are often exacerbated. Mechanical vibrations caused by cooling systems or nearby

https://doi.org/10.1017/hpl.2025.19 Published online by Cambridge University Press

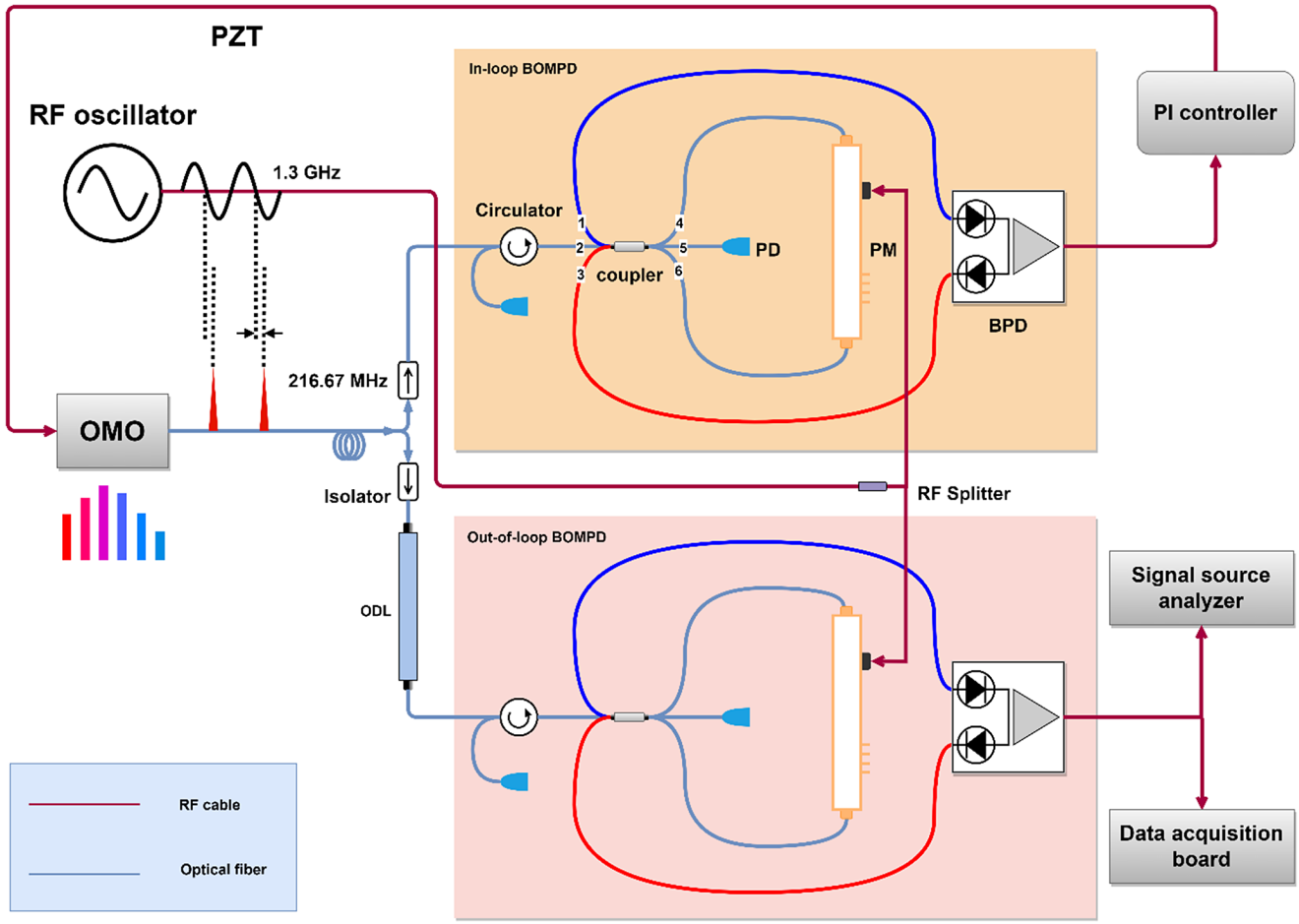

Figure 3. Experimental setup for in-loop phase locking and out-of-loop relative jitter measurement. ODL, optical delay line; PM, phase modulator; PZT, piezoelectric transducer; PD, photodiode; BPD, balanced photodetector.

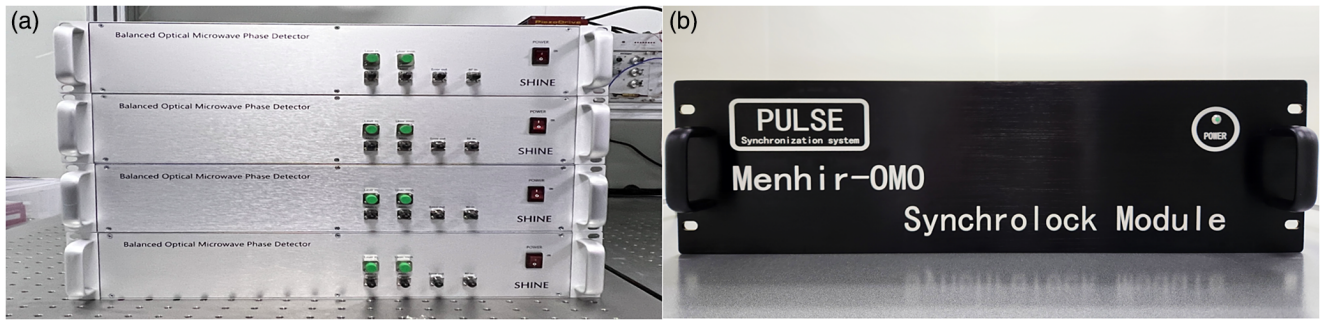

Figure 4. (a) 3×3 based optical to microwave phase detector; (b) OMO electronic synchrolock module for SHINE.

machinery can further compound timing instability by introducing minute strains along the fiber[54]. To mitigate these influences, the development and refinement of a fiber length stabilization system is crucial. Such a system must compensate for environmental changes in real-time, maintaining the precision of time transfer through active feedback mechanisms, thereby ensuring stable femtosecond synchronization throughout the optical fiber link[55–58].

4.1. Fiber length stabilizer

The following section introduces the fundamental principles and design of the FLS, as illustrated in Figure 6. The optical reference pulses are transmitted through the fiber link to remote devices requiring synchronization. Upon reaching the end of the fiber link, a portion of the laser pulses are reflected back to the input end by a partially reflecting

https://doi.org/10.1017/hpl.2025.19 Published online by Cambridge University Press

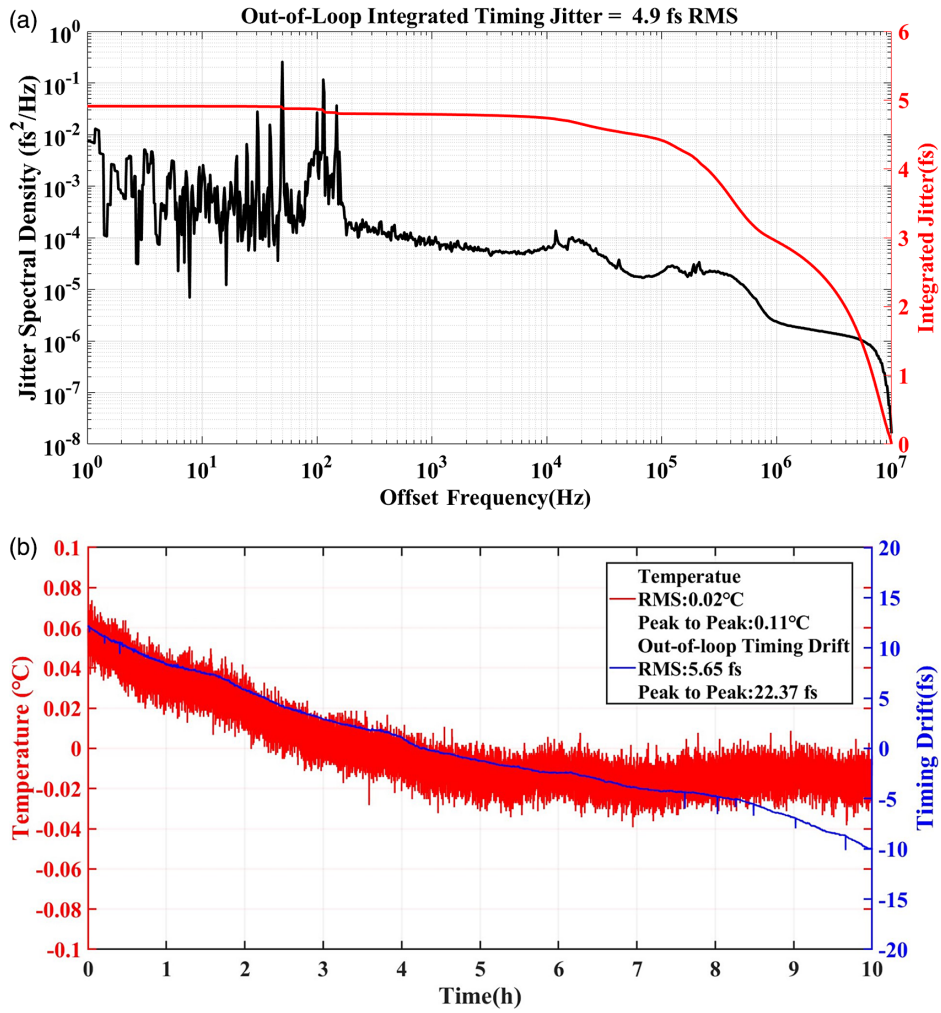

Figure 5. (a) Jitter spectral density (black) and the corresponding integrated timing jitter (red) between RF-signal and phase-locked OMO measured by the out-of-loop phase detector for the frequency offset ranging from 10 Hz to 10 MHz; (b) long-term stability measurement over 10 h.

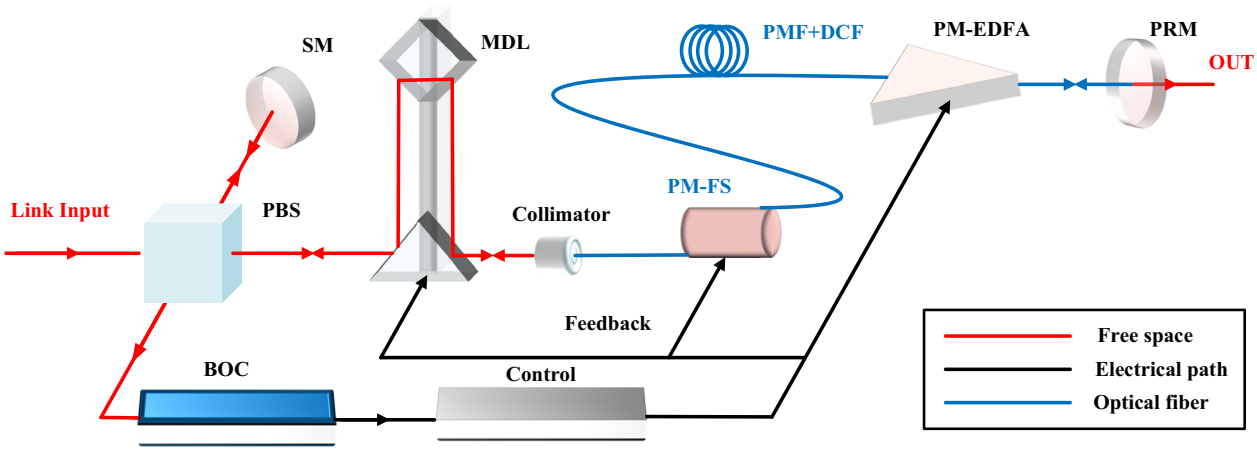

Figure 6. Typical fiber link stabilization setup. SM, silver mirror; PRM, partially reflecting fiber mirror; MDL, motorized delay line; PM-FS, polarization-maintaining fiber stretcher; PM-EDFA, polarization-maintaining erbium-doped optical fiber amplifier; PMF, polarization-maintaining fiber; DCF, dispersion-compensating fiber.

https://doi.org/10.1017/hpl.2025.19 Published online by Cambridge University Press

Figure 7. Fiber length stabilizer at SHINE.

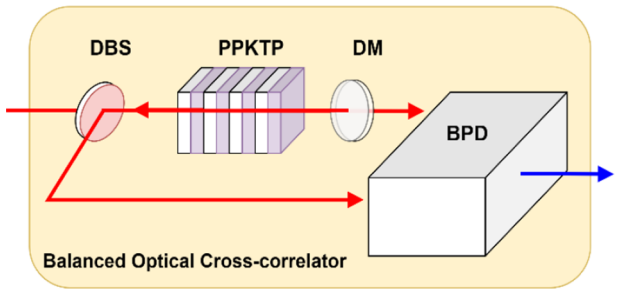

Figure 8. Schematic of balanced optical cross-correlator based on PPKTP crystal. DBS, dichroic beam splitter; DM, dichroic mirror; PPKTP, periodically poled $KTiOPO_4$.

mirror, while the remaining pulses are used for synchronization purposes at the remote station. At the input of the link, the reflected laser pulses are combined with the pulses emitted by OMO. A single-color BOC[55,56] detects propagation delay fluctuations in the fiber link with high resolution and generates an error voltage. A proportional–integral–derivative (PID) controller adjusts the phase error by modulating a piezoelectric-based fiber stretcher to correct rapid timing changes in the fiber link, thereby achieving phase-stable control of the transmitted signal. Additionally, a wide-range optical delay line is introduced to further compensate for larger drifts when the fiber stretcher reaches its limit. This ensures precise synchronization and stability of the transmitted optical reference.

All fiber links in SHINE are constructed using PMFs and dispersion-compensating fibers (DCFs) to mitigate the effects of polarization mode dispersion, which can degrade signal quality over long distances. Additionally, the link integrates a bidirectional erbium-doped fiber amplifier (EDFA) to enhance the pulse energy in the cross-correlator and provide sufficient power for the link output required for remote synchronization. This comprehensive approach enables the FLS to provide stable and precise time transfer across the entire fiber link, ensuring the reliable synchronization necessary for high-precision applications in the SHINE facility. The actual module used for SHINE is shown in Figure 7.

4.2. Balanced optical cross-correlator

As a critical component of the FLS, the timing detection device's resolution significantly impacts the overall precision of the FLS. Due to its high phase detection sensitivity and femtosecond-level precision, the BOC is widely adopted in FLS systems. In 2007, Kim and colleagues demonstrated the effectiveness of a self-aligned BOC, based on a single periodically poled $KTiOPO_4$ (PPKTP) crystal, for stabilizing a 310-m optical fiber link. This setup achieved long-term timing stability with an impressive accuracy of 10 fs, setting a benchmark in timing link stabilization for large-scale scientific facilities[53]. The basic structure of typical BOC is illustrated in Figure 8. In this setup, a dichroic beam splitter (DBS) guides two orthogonally polarized input pulses into the PPKTP crystal, generating a sum-frequency generation (SFG) component. This SFG component is directed through a dichroic mirror and detected by the first photodiode of a balanced photodetector (BPD). The intensity of the SFG component depends on the timing of the input pulses. Simultaneously, the two input pulse trains at the fundamental frequency are reflected back into the crystal, where they generate a second SFG component. This second SFG component is separated by the DBS and detected by the second photodiode of the BPD. The BPD provides a voltage signal proportional to the timing jitter between the pulses by measuring the difference in sum-frequency power between the forward and reverse channels.

Due to the phase-matching bandwidth of approximately 100 nm around 1550 nm, PPKTP crystals are particularly suitable for cross-correlator schemes at this wavelength[53,59,60]. However, the SFG conversion efficiency of PPKTP crystals is relatively low. In addition, the requirement for orthogonal polarization between the reference pulse and the round-trip pulse further limits the phase detection sensitivity of this scheme.

We propose and validate an all-optical cross-correlation phase stabilization device that utilizes a periodically poled lithium niobate (PPLN) crystal, which offers higher SFG conversion efficiency compared to PPKTP crystals. By employing a balanced structure, we suppress common-mode noise in the sum-frequency optical path, thereby enhancing the signal-to-noise ratio (SNR). In addition, we simplify the structure by using a dichroic coating on the exit surface of the crystal instead of a dichroic mirror. In this study, our novel FLS demonstrated an ultra-low integrated timing jitter of 1.3 fs within the 10 Hz–10 MHz range during experiments. Over a period exceeding 24 h, the FLS achieved excellent long-term stability of 4.8 fs (see Figure 9). We believe that this research can provide high-quality and long-term stable reference pulses for SHINE.

https://doi.org/10.1017/hpl.2025.19 Published online by Cambridge University Press

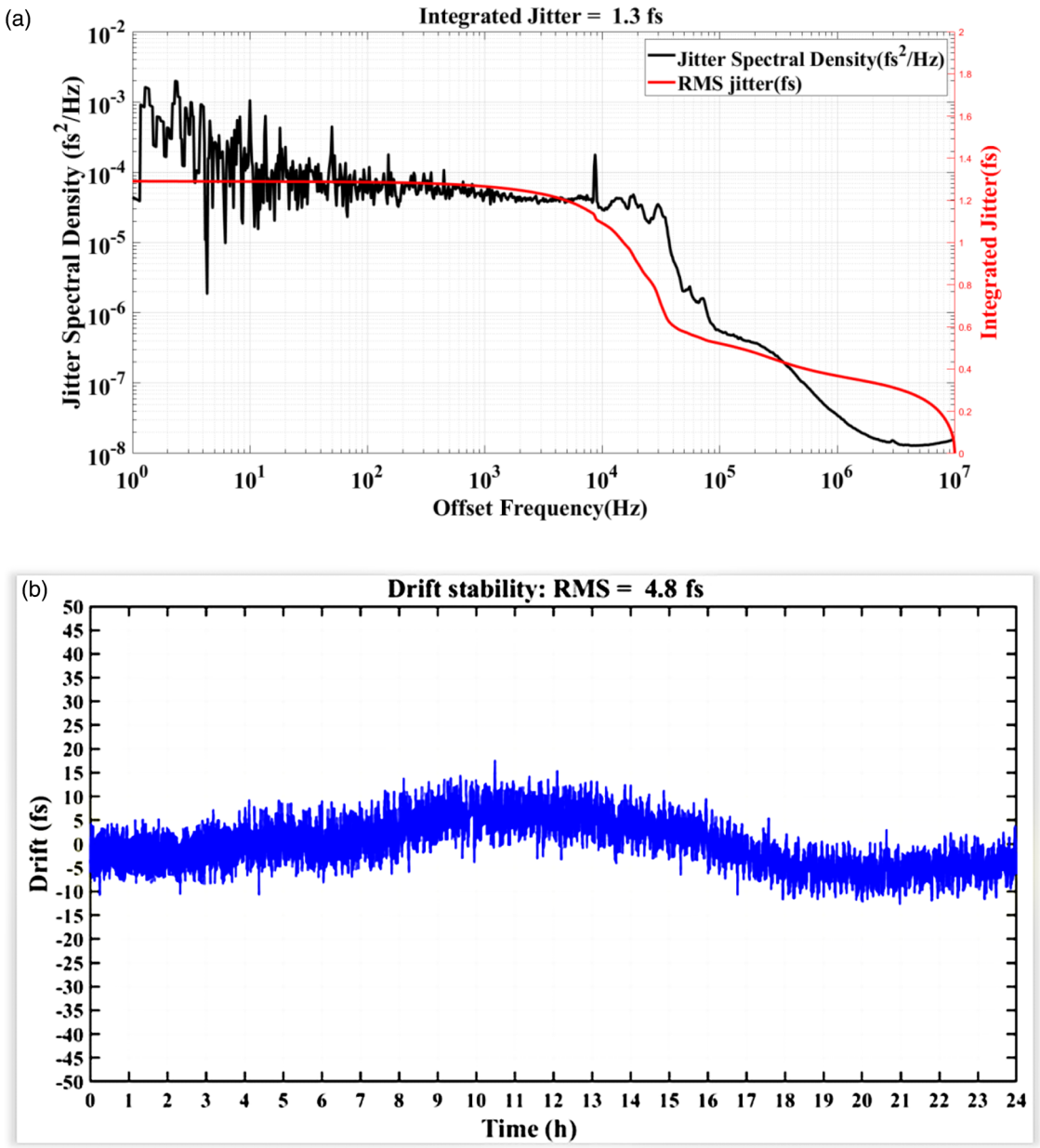

Figure 9. (a) Measured spectral timing jitter density; the integrated RMS jitter from 10 Hz to 10 MHz is 1.3 fs. (b) Long-term stability measurement; the RMS jitter over 24 h is 4.8 fs.

5. External laser-to-laser synchronization

A fundamental characteristic of femtosecond optical synchronization systems using optical pulses is their ability to synchronize external laser systems to an OMO through all-optical techniques. The BOC has proven to be an excellent solution for achieving laser-to-laser synchronization[33,53,61]. Depending on the method used, it can achieve detection resolutions in the femtosecond and even attosecond range. Unlike the method described in the fiber-stabilized link, where the BOC measures the phase difference from the same laser with identical center wavelengths, external lasers (such as seed lasers and pump lasers) often have different center wavelengths. Therefore, structural adjustments are necessary to accommodate these differences. To distinguish from the previously mentioned BOC, we use TC-BOC to describe the laser-to-laser synchronization scheme for optical subsystems. This method ensures tight synchronization of two optical pulse trains at different wavelengths[15,31].

The schematic of this device is shown in Figure 10. The reference pulses from the fiber link and the pulse output from another external laser are combined using a dichroic beam combiner (DBC) and directed into a barium borate (BBO) crystal. Here, the two input pulse trains generate a forward SFG signal. Similar to the previous monochromatic BOC, the forward SFG signal is separated by the dichroic mirror and detected by the balanced photodetector. Unlike

https://doi.org/10.1017/hpl.2025.19 Published online by Cambridge University Press

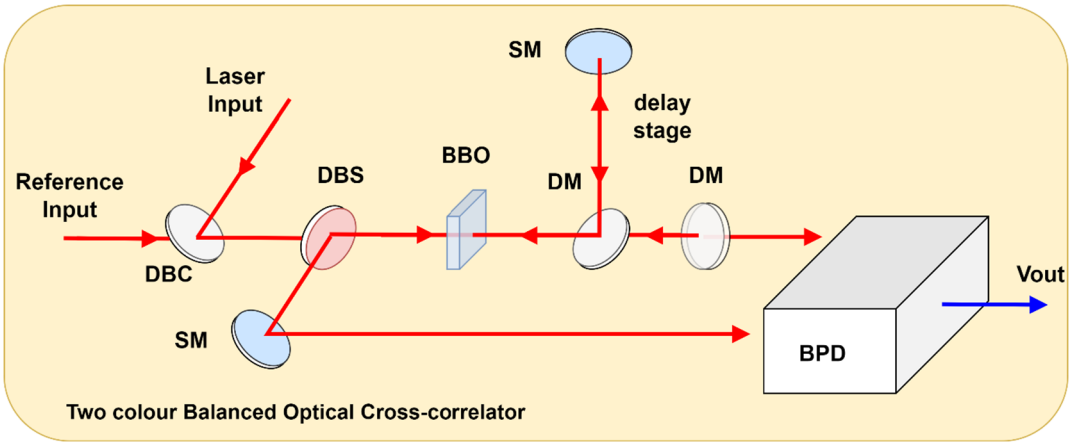

Figure 10. Schematic of a two-color optical cross-correlator. DBC, dichroic beam combiner; DBS, dichroic beam splitter; BBO, beta barium borate crystal; DM, dichroic mirror; SM, sliver mirror.

the previous scheme, the reflected pulse train is introduced with a specific differential group delay through an adjustable optical delay line and passes through the BBO crystal a second time to generate a reverse SFG signal. By detecting the difference between the two SFG signals using the BPD, the output voltage signal can accurately measure the timing error between the two input laser pulse trains.

In our experiment, we used the TC-BOC to synchronize two different laser pulse trains. The master laser was a commercial mode-locked laser from Menhir Photonics, operating at a central wavelength of 1550 nm with a repetition rate of 238 MHz. The slave laser was an experimental pulse train from the SHINE Seed Laser Laboratory, operating at a central wavelength of 800 nm with a repetition rate of 79.33 MHz. Using an out-of-loop TC-BOC with the same structure, we determined the synchronization performance between the seed laser and the mode-locked laser. Figure 11 shows the measured single-sideband phase noise, indicating that our TC-BOC achieved an out-of-loop jitter of 8.7 fs RMS over a bandwidth from 10 Hz to 10 MHz. In addition, a notable 1.2 fs RMS timing drift over 8 h is measured.

Based on its excellent performance, the TC-BOC will be widely used in SHINE to synchronize various remote optical subsystems. The integrated laser-to-laser synchronization module is shown in Figure 12. The combined implementation of FLS and TC-BOC effectively minimizes both fast jitter and long-term drift, ensuring femtosecond-level stability over extended operation periods. In addition, considering that additional drift and jitter can easily be introduced into the beamline in photoelectric cathodes or pump-probe detection lasers, we also plan to apply the TC-BOC to measure and compensate for timing variations of laser pulses upon arrival at the laboratory. This setup measures and corrects for timing variations upon laser pulse arrival, providing a final layer of drift compensation at the point of use.

6. Conclusions

We presented the design and implementation of SHINE's femtosecond-level synchronization system, which delivers high-precision synchronization solutions across a large-scale XFEL facility. This system, based primarily on optical methods, ensures robust performance and is comparable in scale and complexity to the synchronization systems of established XFEL facilities like the European XFEL. SHINE's system combines key technologies, such as OMO, FLS and advanced phase detection via 3×3 BOMPD configurations, to meet stringent synchronization requirements.

The architecture of SHINE's synchronization system offers several advantages. Its centralized optical-based structure improves signal integrity and phase noise resilience across the facility, from the accelerator to the experimental end stations. In addition, the fiber-based reference distribution links benefit from temperature stabilization measures and dispersion compensation, which compensate for environmental drift over long distances, even in challenging accelerator tunnel conditions. The deployment of a Sagnac-based 3×3 coupler in the BOMPD further simplifies phase detection, eliminating complex biasing components and achieving femtosecond resolution with sufficient stability.

Key components have been rigorously tested in laboratory conditions and demonstrated consistent femtosecond-level synchronization precision, validating their readiness for full-scale implementation at SHINE. Table 1 summarizes the performance achieved, confirming the system's potential to meet the demands of a high-repetition-rate XFEL.

With the advanced synchronization system under development, femtosecond-level synchronization across various subsystems is achievable, positioning SHINE as a leading XFEL facility for ultrafast scientific research applications. Future efforts will focus on system integration and long-term stability under operational conditions, with potential

https://doi.org/10.1017/hpl.2025.19 Published online by Cambridge University Press

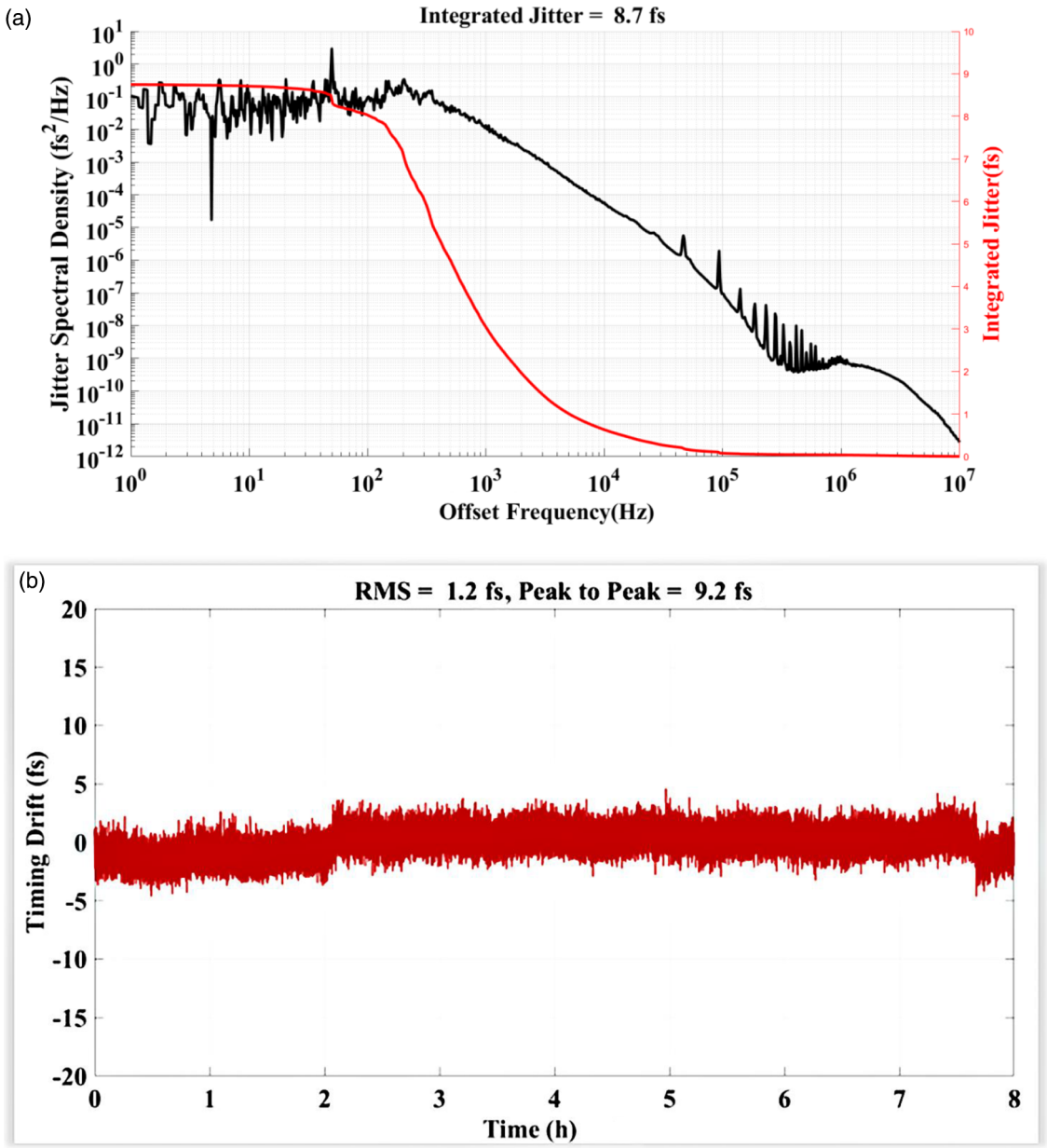

Figure 11. Measurement result of laser-to-laser synchronization between mode-locked laser and seed laser using TC-BOC: (a) jitter spectral density and integrated timing jitter; (b) long-term drift measurement.

Figure 12. Laser-to-laser synchronization module in SHINE.

https://doi.org/10.1017/hpl.2025.19 Published online by Cambridge University Press

Table 1. Critical synchronization parameters in SHINE.

Process	Subsystem/Technique	Achieved precision
Laser-to-RF synchronization	3×3 BOMPD with Sagnac loop	4.9 fs, 10 Hz to 10 MHz jitter
Fiber link stabilization	Piezo stretchers and optical delay lines	1.3 fs, 10 Hz to 10 MHz jitter 4.8 fs, 24 h drift
External laser-to-laser synchronization	TC-BOC for laser-to-laser synchronization	8.7 fs, 10 Hz to 10 MHz jitter 1.2 fs, 8 h drift

expansions for further enhancing drift control and synchronization precision.

Acknowledgement

This work is supported by the National Natural Science Foundation of China (Nos. 12105348 and 12275341) and the SHINE project (National Major Scientific and Technological Infrastructure, No. NDRC [2017]825).

References

1. T. Shintake, H. Tanaka, T. Hara, T. Tanaka, K. Togawa, M. Yabashi, Y. Otake, Y. Asano, T. Bizen, and T. Fukui, Nat. Photonics **2**, 555 (2008).
2. P. Emma, R. Akre, J. Arthur, R. Bionta, C. Bostedt, J. Bozek, A. Brachmann, P. Bucksbaum, R. Coffee, and F.-J. Decker, Nat. Photonics **4**, 641 (2010).
3. W. Ackermann, G. Asova, V. Ayvazyan, A. Azima, N. Baboi, J. Bähr, V. Balandin, B. Beutner, A. Brandt, A. Bolzmann, R. Brinkmann, O. I. Brovko, M. Castellano, P. Castro, L. Catani, E. Chiadroni, S. Choroba, A. Cianchi, J. T. Costello, D. Cubaynes, J. Dardis, W. Decking, H. Delsim-Hashemi, A. Delserieys, G. Di Pirro, M. Dohlus, S. Düsterer, A. Eckhardt, H. T. Edwards, B. Faatz, J. Feldhaus, K. Flöttmann, J. Frisch, L. Fröhlich, T. Garvey, U. Gensch, C. Gerth, M. Görler, N. Golubeva, H. J. Grabosch, M. Grecki, O. Grimm, K. Hacker, U. Hahn, J. H. Han, K. Honkavaara, T. Hott, M. Hüning, Y. Ivanisenko, E. Jaeschke, W. Jalmuzna, T. Jezynski, R. Kammering, V. Katalev, K. Kavanagh, E. T. Kennedy, S. Khodyachykh, K. Klose, V. Kocharyan, M. Körfer, M. Kollewe, W. Koprek, S. Korepanov, D. Kostin, M. Krassilnikov, G. Kube, M. Kuhlmann, C. L. S. Lewis, L. Lilje, T. Limberg, D. Lipka, F. Löhl, H. Luna, M. Luong, M. Martins, M. Meyer, P. Michelato, V. Miltchev, W. D. Möller, L. Monaco, W. F. O. Müller, A. Napieralski, O. Napoly, P. Nicolosi, D. Nölle, T. Nuñez, A. Oppelt, C. Pagani, R. Paparella, N. Pchalek, J. Pedregosa-Gutierrez, B. Petersen, B. Petrosyan, G. Petrosyan, L. Petrosyan, J. Pflüger, E. Plönjes, L. Poletto, K. Pozniak, E. Prat, D. Proch, P. Pucyk, P. Radcliffe, H. Redlin, K. Rehlich, M. Richter, M. Roehrs, J. Roensch, R. Romaniuk, M. Ross, J. Rossbach, V. Rybnikov, M. Sachwitz, E. L. Saldin, W. Sandner, H. Schlarb, B. Schmidt, M. Schmitz, P. Schmüser, J. R. Schneider, E. A. Schneidmiller, S. Schnepp, S. Schreiber, M. Seidel, D. Sertore, A. V. Shabunov, C. Simon, S. Simrock, E. Sombrowski, A. A. Sorokin, P. Spanknebel, R. Spesyvtsev, L. Staykov, B. Steffen, F. Stephan, F. Stulle, H. Thom, K. Tiedtke, M. Tischer, S. Toleikis, R. Treusch, D. Trines, I. Tsakov, E. Vogel, T. Weiland, H. Weise, M. Wellhöffer, M. Wendt, I. Will, A. Winter, K. Wittenburg, W. Wurth, P. Yeates, M. V. Yurkov, I. Zagorodnov, and K. Zapfe, Nat. Photonics **1**, 336 (2007).
4. T. Liu, N. Huang, H. Yang, Z. Qi, K. Zhang, Z. Gao, S. Chen, C. Feng, W. Zhang, and H. Luo, Front. Phys. **11**, 1172368 (2023).
5. C. Pellegrini and J. Stöhr, Nucl. Instrum. Methods Phys. Res. Sect. A **500**, 33 (2003).
6. H. N. Chapman and J. C. H. Spence, Acta Crystallogr. A Found. Adv. **66**, S8 (2010).
7. L. Redecke, K. Nass, D. P. DePonte, T. A. White, D. Rehders, A. Barty, F. Stellato, M. Liang, T. R. M. Barends, S. Boutet, G. J. Williams, M. Messerschmidt, M. M. Seibert, A. Aquila, D. Arnlund, S. Bajt, T. Barth, M. J. Bogan, C. Caleman, T.-C. Chao, R. B. Doak, H. Fleckenstein, M. Frank, R. Fromme, L. Galli, I. Grotjohann, M. S. Hunter, L. C. Johansson, S. Kassemeyer, G. Katona, R. A. Kirian, R. Koopmann, C. Kupitz, L. Lomb, A. V. Martin, S. Mogk, R. Neutze, R. L. Shoeman, J. Steinbrener, N. Timneanu, D. Wang, U. Weierstall, N. A. Zatsepin, J. C. H. Spence, P. Fromme, I. Schlichting, M. Duszenko, C. Betzel, and H. N. Chapman, Science **339**, 227 (2013).
8. B. Rudek, S. K. Son, L. Foucar, S. W. Epp, B. Erk, R. Hartmann, M. Adolph, R. Andritschke, A. Aquila, N. Berrah, C. Bostedt, J. Bozek, N. Coppola, F. Filsinger, H. Gorke, T. Gorkhover, H. Graafsma, L. Gumprecht, A. Hartmann, G. Hauser, S. Herrmann, H. Hirsemann, P. Holl, A. Hömke, L. Journel, C. Kaiser, N. Kimmel, F. Krasniqi, K. U. Kühnel, M. Matysek, M. Messerschmidt, D. Miesner, T. Möller, R. Moshammer, K. Nagaya, B. Nilsson, G. Potdevin, D. Pietschner, C. Reich, D. Rupp, G. Schaller, I. Schlichting, C. Schmidt, F. Schopper, S. Schorb, C. D. Schröter, J. Schulz, M. Simon, H. Soltau, L. Strüder, K. Ueda, G. Weidenspointner, R. Santra, J. Ullrich, A. Rudenko, and D. Rolles, Nat. Photonics **6**, 858 (2012).
9. S. M. Vinko, O. Ciricosta, B. I. Cho, K. Engelhorn, H. K. Chung, C. R. D. Brown, T. Burian, J. Chalupsky, R. W. Falcone, C. Graves, V. Hájková, A. Higginbotham, L. Juha, J. Krzywinski, H. J. Lee, M. Messerschmidt, C. D. Murphy, Y. Ping, A. Scherz, W. Schlotter, S. Toleikis, J. J. Turner, L. Vysin, T. Wang, B. Wu, U. Zastrau, D. Zhu, R. W. Lee, P. A. Heimann, B. Nagler, and J. S. Wark, Nature **482**, 59 (2012).
10. J. Kim, J. A. Cox, J. Chen, and F. X. Kaertner, Nat. Photonics **2**, 733 (2008).
11. K. Şafak, M. Xin, M. Y. Peng, and F. X. Kärtner, Sci. Rep. **8**, 11948 (2018).
12. M. Xin, K. Safak, and F. X. Kaertner, Optica **5**, 1564 (2018).
13. M. Xin, K. Şafak, M. Y. Peng, P. T. Callahan, A. Kalaydzhyan, W. Wang, K. Shtyrkova, Q. Zhang, S.-H. Chia, and B. Jones, Nucl. Instrum. Methods Phys. Res. Sect. A **907**, 169 (2018).
14. J. Kim, F. Ilday, F. Kärtner, O. Mücke, M. Perrott, W. Graves, D. Moncton, and T. Zwart, in *Proceedings of the FEL Conference* (2004), p. 339.
15. S. Schulz, I. Grguraš, C. Behrens, H. Bromberger, J. Costello, M. K. Czwalinna, M. Felber, M. Hoffmann, M. Ilchen, and H. Liu, Nat. Commun. **6**, 5938 (2015).
16. M. Felber, L. Butkowski, M. Czwalinna, M. Fenner, C. Gerth, M. Heuer, M. Killenberg, T. Lamb, U. Mavrič, and J. Mueller, in *Proceedings of the 37th International Free Electron Laser Conference* (2015), p. 115.
17. T. Lamb, M. Czwalinna, M. Felber, C. Gerth, T. Kozak, J. Müller, H. Schlarb, S. Schulz, C. Sydlo, and M. Titberidze, in *Proceedings of the 10th International Particle Accelerator Conference* (2019), p. 3835.

https://doi.org/10.1017/hpl.2025.19 Published online by Cambridge University Press

18. S. Schulz, M. Czwalinna, M. Felber, M. Fenner, C. Gerth, T. Kozak, T. Lamb, B. Lautenschlager, F. Ludwig, and U. Mavric, in *Proceedings of the 39th International Free Electron Laser Conference* (2019), p. 318.
19. J. Byrd, G. Huang, R. Wilcox, B. Hill, and A. Fry, in *Proceedings of the 3rd International Particle Accelerator Conference* (2012), p. 2176.
20. K. Şafak, S. Droste, H. P. H. Cheng, A. Dai, K. Gumerlock, A. Berlin, S. Bhat, M. Neuhaus, J. Paradowski, and F. Okrent, in *CLEO: Science and Innovations* (2020), paper SM2N.5.
21. E. Prat, R. Abela, M. Aiba, A. Alarcon, J. Alex, Y. Arbelo, C. Arrell, V. Arsov, C. Bacellar, and C. Beard, Nat. Photonics **14**, 748 (2020).
22. K. Şafak, H. P. H. Cheng, A. Dai, M. Kaiser, V. Arsov, A. Berlin, E. Cano, W. Nasimzada, M. Neuhaus, and P. Schiepel, in *CLEO: Applications and Technology* (2019), paper JTh2A.100.
23. T. Ishikawa, H. Aoyagi, T. Asaka, Y. Asano, N. Azumi, T. Bizen, H. Ego, K. Fukami, T. Fukui, and Y. Furukawa, Nat. Photonics **6**, 540 (2012).
24. E. Allaria, R. Appio, L. Badano, W. Barletta, S. Bassanese, S. Biedron, A. Borga, E. Busetto, D. Castronovo, and P. Cinquegrana, Nat. Photonics **6**, 699 (2012).
25. H.-S. Kang, C.-K. Min, H. Heo, C. Kim, H. Yang, G. Kim, I. Nam, S. Y. Baek, H.-J. Choi, and G. Mun, Nat. Photonics **11**, 708 (2017).
26. Z. Zhao, D. Wang, Q. Gu, L. Yin, M. Gu, Y. Leng, and B. Liu, Appl. Sci. **7**, 607 (2017).
27. L. Feng, W. Zhang, J. Wang, C. Li, X. Wang, and B. Liu, in *Proceedings of the 12th International Particle Accelerator Conference* (2021), p. 4406.
28. C. Sydlo, F. Zummack, J. Mueller, M. Felber, M. Czwalinna, C. Gerth, H. Schlarb, and G. S. Jablonski, in *Proceedings of the 37th International Free Electron Laser Conference* (2015), p. 669.
29. J.-G. Wang and B. Liu, Nucl. Sci. Tech. **30**, 113 (2019).
30. F. Löhl, V. Arsov, M. Felber, K. Hacker, W. Jalmuzna, B. Lorbeer, F. Ludwig, K. H. Matthiesen, H. Schlarb, B. Schmidt, P. Schmüser, S. Schulz, J. Szewinski, A. Winter, and J. Zemella, Phys. Rev. Lett. **104**, 144801 (2010).
31. H. Li, L. J. Chen, H. P. H. Cheng, J. E. May, S. Smith, K. Muehlig, A. Uttamadoss, J. C. Frisch, A. R. Fry, F. X. Kärtner, and P. H. Bucksbaum, Opt. Lett. **39**, 5325 (2014).
32. V. Arsov, M. Felber, F. Löhl, B. Lorbeer, F. Ludwig, K. Matthiesen, H. Schlarb, B. Schmidt, and A. W. D. Elektronen-Synchrotron, in *Proceedings of the 11th European Particle Accelerator Conference* (2008), p. 3366.
33. T. Schibli, J. Kim, O. Kuzucu, J. Gopinath, S. Tandon, G. Petrich, L. Kolodziejski, J. Fujimoto, E. Ippen, and F. Kaertner, Opt. Lett. **28**, 947 (2003).
34. A. J. Benedick, J. G. Fujimoto, and F. X. Kärtner, Nat. Photonics **6**, 97 (2012).
35. M. C. Divall, M. Kaiser, S. Hunziker, C. Vicario, B. Beutner, T. Schietinger, M. Lüthi, M. Pedrozzi, and C. P. Hauri, Nucl. Instrum. Methods Phys. Res. Sect. A **735**, 471 (2014).
36. M. Csatari Divall, P. Mutter, E. J. Divall, and C. P. Hauri, Opt. Express **23**, 29929 (2015).
37. P. Sigalotti, P. Cinquegrana, A. Demidovich, R. Ivanov, I. Nikolov, G. Kurdi, and M. Danailov, Proc. SPIE **8778**, 87780Q (2013).
38. B. Ning, S. Y. Zhang, D. Hou, J. T. Wu, Z. B. Li, and J. Y. Zhao, Sci. Rep. **4**, 5109 (2014).
39. T. K. Kim, Y. Song, K. Jung, C. Kim, H. Kim, C. H. Nam, and J. Kim, Opt. Lett. **36**, 4443 (2011).
40. J. Wang, B. Liu, and B. Wu, in *12th International Beam Instrumentation Conference* (2023), p. 151.
41. J. J. McFerran, E. N. Ivanov, A. Bartels, G. Wilpers, C. W. Oates, S. A. Diddams, and L. Hollberg, Electron. Lett. **41**, 1 (2005).
42. T. M. Fortier, F. Quinlan, A. Hati, C. Nelson, J. A. Taylor, Y. Fu, J. Campbell, and S. A. Diddams, Opt. Lett. **38**, 1712 (2013).
43. M. Titberidze, M. Felber, T. Lamb, R. Loch, C. Sydlo, and H. Schlarb, J. Phys. Conf. Ser. **874**, 012085 (2017).
44. W. Zhang, T. Li, M. Lours, S. Seidelin, G. Santarelli, and Y. Le Coq, Appl. Phys. B **106**, 301 (2012).
45. J. Kim, F. X. Kartner, and F. Ludwig, Opt. Lett. **31**, 3659 (2006).
46. M. Y. Peng, A. Kalaydzhyan, and F. X. Kärtner, Opt. Express **22**, 27102 (2014).
47. K. Jung and J. Kim, Opt. Lett. **37**, 2958 (2012).
48. J. Kim, F. X. Kärtner, and M. H. Perrott, Opt. Lett. **29**, 2076 (2004).
49. K. Jung and J. Kim, in *IEEE International Frequency Control Symposium* (2012), p. 1.
50. W. Y. Zhang, X. Q. Liu, L. Feng, T. H. Lan, X. T. Wang, and B. Liu, Nucl. Sci. Tech. **29**, 91 (2018).
51. C.-G. Jeon, Y. Na, B.-W. Lee, and J. Kim, Opt. Lett. **43**, 3997 (2018).
52. J.-W. Kim, "High-precision optical and microwave signal synthesis and distribution", PhD Thesis (Massachusetts Institute of Technology, 2007).
53. J. Kim, J. Chen, Z. Zhang, F. N. C. Wong, F. X. Kaertner, F. Loehl, and H. Schlarb, Opt. Lett. **32**, 1044 (2007).
54. W. Thomes, F. LaRocca, R. Switzer, M. Ott, R. Chuska, and S. Macmurphy, Proc. SPIE **7070**, 70700A (2008).
55. K. Safak, M. Xin, M. Y. Peng, P. T. Callahan, and F. X. Kärtner, in *IEEE International Frequency Control Symposium* (2014), p. 1.
56. M. Xin, K. Şafak, M. Y. Peng, P. T. Callahan, and F. X. Kärtner, Opt. Express **22**, 14904 (2014).
57. K. Şafak, M. Xin, P. Callahan, M. Peng, and F. Kärtner, Struct. Dyn. **2**, 041715 (2015).
58. K. Safak, M. Xin, Q. Zhang, S.-H. Chia, O. D. Muecke, and F. X. Kaertner, Opt. Express **24**, 21752 (2016).
59. A. H. Nejadmalayeri, F. N. Wong, T. D. Roberts, P. Battle, and F. X. Kärtner, Opt. Lett. **34**, 2522 (2009).
60. P. T. Callahan, K. Safak, P. Battle, T. D. Roberts, and F. X. Kärtner, Opt. Express **22**, 9749 (2014).
61. M. Xin, K. Şafak, M. Y. Peng, A. Kalaydzhyan, W.-T. Wang, O. D. Mücke, and F. X. Kärtner, Light Sci. Appl. **6**, e16187 (2017).

https://doi.org/10.1017/hpl.2025.19 Published online by Cambridge University Press